Absence of spin Hall magnetoresistance in Pt/(CoNi)$_n$ multilayers

Yongwei Cui [1], Xiaoyu Feng,[1] Qihan Zhang,[1] Hengan Zhou,[2] Wanjun Jiang,[2] Jiangwei Cao [1],[1]
Desheng Xue,[1] and Xiaolong Fan[1,*]

[1]*Key Laboratory for Magnetism and Magnetic Materials of the Ministry of Education, Lanzhou University,
Lanzhou 730000, People's Republic of China*

[2]*State Key Laboratory of Low-Dimensional Quantum Physics and Department of Physics, Tsinghua University, Beijing 100084, China*

We have systematically studied the magnetoresistance effect in Pt/(CoNi)$_n$ multilayers featured with perpendicular magnetic anisotropy and fcc (111) texture. Angular dependence of the magnetoresistance, including high-order cosine terms, was found in the plane perpendicular to the electrical current, which can be attributed to the geometrical size effects and the anisotropic interface magnetoresistance effect. However, the contribution from spin Hall magnetoresistance (SMR) is absent. The spin Hall angle of Pt was evaluated by spin-torque ferromagnetic resonance measurements, and the theoretical magnitude of SMR in our samples was estimated to be one order higher than the accuracy of our experiments. The absence of SMR in our multilayers indicates that the Elliott-Yafet spin relaxation of itinerant electrons in the ferromagnetic metal is crucial when studying the spin transport in all-metallic heterostructures.

I. INTRODUCTION

Spin Hall magnetoresistance (SMR) refers to the anisotropic absorption of spin current with respect to the relative orientation of magnetization in the heavy-metal (HM)/ferromagnet bilayers, by a change in HM resistance with the direction of magnetization [1–3]. Because SMR essentially reflects the interaction between spin current and local magnetic moment, it has become a powerful tool for studying spin-orbit coupling in magnetic heterostructures. For examples, SMR can be used to determine the spin Hall angle, spin-diffusion length in HM, and interface spin-mixing conductance [2–5], even interfacial spin-orbit coupling can be studied by spin-orbit MR [6]. In addition, SMR can also be used to monitor the directions of the Néel order in antiferromagnetic materials by means of highly sensitive electrical measurements [7–10].

An SMR model was first proposed in the heterostructure of HMs and ferromagnetic insulators (FMI) [2,11,12], and was then adopted to study the spin-dependent transport behaviors in all-metallic heterostructures [4,5,13]. Compared with HM/FMI, the SMR effect in an HM/ferromagnetic metal (FM) bilayer is more complicated. Based on previous theoretical proposals, the absorption of the longitudinal spin current by the FM layer [5], the spin current generated by the FM layer [14], and the anomalous Hall effect of the FM layer [4,15,16] should also be considered. More importantly, although the appearance of the magnetoresistance effect in the plane perpendicular to the charge current (i.e., the *yz* plane) can be used to distinguish SMR from traditional anisotropic magnetoresistance (AMR), the ordered arrangement of grains in

FMs and the interfacial symmetry breaking could also lead to the appearance of the magnetoresistance effect in that plane [17–19]. For example, Kobs *et al.* observed distinct magnetoresistance in the *yz* plane in a Pt/Ni/Pt system, but found that the contribution of SMR could almost be ignored [20]. The absence of SMR in all-metallic heterostructure brings the other complicacy which implies either the spin-orbit coupling is quite weak, or the SMR model in HM/FMI cannot be directly adopted. Hence, it is necessary to revisit the magnitude of SMR in HM/FM bilayers.

In the present paper, we employed (CoNi)$_n$ multilayers with perpendicular magnetic anisotropy (PMA) to study SMR effect. The difference from other films with PMA such as Ta/CoFeB/MgO is their artificially tunable PMA over a significantly wider range of magnetic thickness [21–23]. Therefore, (CoNi)$_n$ multilayers are desirable spintronics materials to study magnetic domain-wall motion and magnetization switching [9,24–26]. In addition, (CoNi) multilayers exhibit moderate intrinsic damping and higher spin polarization [27–29] compared with other bulk PMA films, enabling to develop better performance spin-torque magnetic random access memories (MRAMs) and data storage applications [30]. However, we found that the magnitude of SMR in Pt/(CoNi)$_n$ is far less than what was predicted theoretically based on the measurements of spin-torque ferromagnetic resonance (ST-FMR), which led us to further explore the mechanism of spin transport in all-metallic magnetic heterostructures.

II. THIN-FILM DEPOSITION AND STRUCTURAL CHARACTERIZATION

In this work, Ta(3)/Pt(10)/[Co(0.3)/Ni(0.4)]$_n$/Ta(3) were deposited onto SiO$_2$/Si substrate by magnetron sputtering at room temperature. The numbers in brackets represent
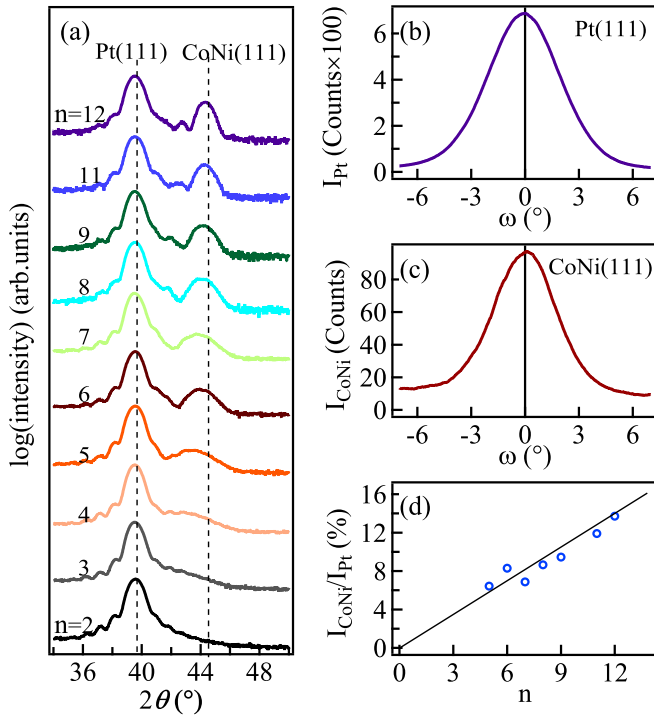
*fanxiaolong@lzu.edu.cn

FIG. 1. (a) Out-of-plane x-ray measurement of Ta(3)/Pt(10)/
[Co(0.3)/Ni(0.4)]$_n$/Ta(3) for *n* ranging from 2 to 12. The dashed
lines at 39.7° and 44.5° represent the expected positions of unstrained
Pt (111) and CoNi (111) peaks, respectively. (b), (c) Rocking curves
around Pt (111) and [Co/Ni]$_{12}$ (111). (d) The blue cycles are the
dependence of the peak intensity ratio of [Co/Ni]$_n$ and Pt on the
number of repetitions *n*. The black line is a straight line through the
origin that was fitted to our results.

the thickness of each layer in nanometer units. *n* = 2, 3, 4,
5, 6, 7, 8, 9, 11, and 12 are the number of repetitions of the
magnetic double layer. The thickness of Pt, Co, and Ni layers
is the optimized choice that the samples show maximum PMA
at a certain repetition number *n*. Moreover, Pt/Co/Ni stacking
order is also favorable to obtain perpendicularly magnetized
CoNi multilayers due to a larger interface anisotropy at Pt/Co
interface compared with Pt/Ni [31]. The Ta in the lower
and upper layers form buffer and protective layers, which
reduce the influence of substrate roughness on the film and
prevent the film from being oxidized. The base pressure of
the main chamber is better than 2×10^{-8} Torr, and the Ar
pressure is maintained at 3×10^{-3} Torr during sputtering. The
static magnetic properties of all the samples were obtained by
vibrating-sample magnetometry, and the crystal structure was
characterized by high-resolution x-ray diffractometry (HR-
XRD) with a Cu $K\alpha$ radiation source. The magnetoresistance
was characterized using the physical property measurement
system (Quantum Design), and ST-FMR test was completed
using a home-built system.

First, we determined the crystal structure and orientation of
all the samples. Figure 1(a) shows the $\theta - 2\theta$ x-ray-diffraction
spectrum of samples with different repetition numbers, where
the dashed lines at 39.7° and 44.5° represent the unstrained
positions of the Pt (111) and CoNi (111) peaks, respectively
[32,33]. For *n* = 2, only Pt (111) peak appears in the range of

34°–50°, and a number of clear secondary diffraction peaks
generated by Laue oscillation can be seen around this peak,
indicating that Pt has a high crystallinity quality in the (111)
orientation and low interface roughness. When *n* > 4, a rel-
atively weak peak appears at 42°–44°. As *n* increases, the
strength of the peak gradually becomes stronger and the peak
position gradually approaches 44.5°. Using Gaussian fitting,
the full width at half maximum of the rocking curves around
the Pt (111) and CoNi (111) reflections can be determined
to be 5.7° and 4.9°, respectively, as shown in Figs. 1(b) and
1(c). This indicates that the Pt and CoNi in the samples have
(111) texture along the normal direction of the film. In order
to illustrate the precise control of the number of repetition, the
ratio of the intensity of CoNi (111) and Pt (111) is shown in
Fig. 1(d). It is evident that a straight line through the zero point
can be used to fit our experimental results (open circles). Thus,
changing the number of repetitions only increases the number
of crystallographic plane participating in Bragg reflection, but
does not affect the crystal structure of each CoNi layer.

To further demonstrate that we have achieved accurate reg-
ulation of CoNi repetition, we also measured the dependence
of PMA on *n*. As shown in Figs. 2(a) and 2(b), the abnormal
Hall resistance curve of *n* = 8 was measured when a magnetic
field was applied out of plane and in plane. The presence of
PMA is evident from square-shaped anomalous Hall effect
(AHE), as shown in Fig. 2(a) [22,34]. In order to obtain the
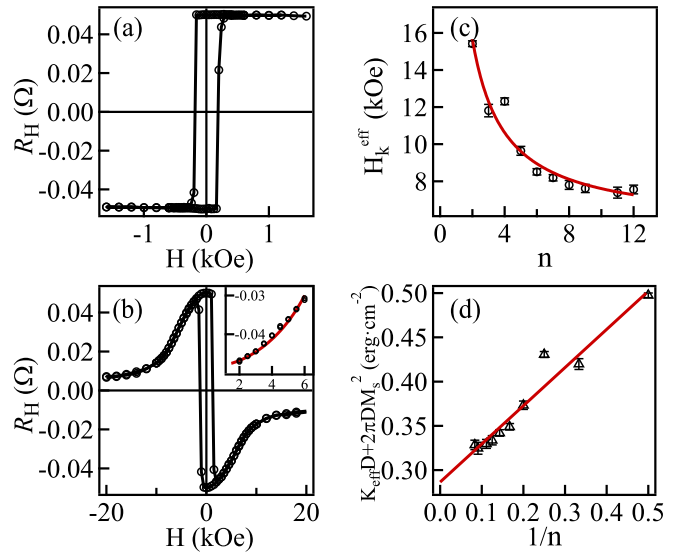exact value of H_k^{eff}, we use the following formula [35]:

FIG. 2. (a), (b) The loops of abnormal Hall resistance when a
magnetic field was applied along the film normal and plane of *n* = 8.
The inset in (b) shows local enlarged data from 1.6 to 6 kOe, and
the curve is the result of fitting using Eq. (1). (c) The black circles
represent the dependence of the effective PMA field on the repetition
number, which can be well fitted by $A/n + B$ (*A* and *B* are constants)
as the curve shows. (d) The triangle represents the perpendicular
anisotropy energy per unit area, and the red line denotes a linear
fitting.

$$\frac{\rho_{xy}(H_x)}{\rho_{xy}(0)} = \sqrt{1 - \left(\frac{H_x}{H_k^{\text{eff}}}\right)^2} \qquad (1)$$

FIG. 3. Magnetoresistance curves of Pt/[Co/Ni]$_n$ structures. (a) Illustration of the Ta/Pt/[Co/Ni]$_n$/Ta sample structure and coordinate system of the experiment. (b) Resistivity ρ vs orientation of magnetization for three samples with different repetitions. The rotation of magnetization **M** is performed in the film plane ($\beta = 90°$, black cycles) and in the plane perpendicular to the current **j** ($\alpha = 90°$, red cycles). (c) Individual $\cos^{2n}\beta$ contributions to $\rho(\beta)$ for $n = 12$. (d) Polar plot of $\rho(\beta)$ for these three samples.

to fit the AHE curve in Fig. 2(b) with the range of $1.6 \sim 6$ kOe. The fitting result is $H_k^{\text{eff}} = 7.6 \pm 0.1$ kOe. Subsequently, the relationship between H_k^{eff} and n can be obtained, as shown in Fig. 2(c). The evolution of H_k^{eff} as a function of layer repetition n suggests dominated interfacial contribution to the strength of PMA [32]. Combined with the method of You *et al.* [22], neglecting the Co and Ni volume anisotropy energies, the average perpendicular anisotropic energy per unit area of each CoNi layer can be written as

$$K_{\text{eff}}D + 2\pi D M_s^2 = K_s^{\text{Co/Ni}} + K_s^{\text{Ni/Co}}$$
$$+ (1/n)\left(K_s^{\text{Pt/Co}} + K_s^{\text{Ni/Ta}} - K_s^{\text{Ni/Co}}\right). \quad (2)$$

In this equation, $K_{\text{eff}} = \frac{H_k^{\text{eff}} M_s}{2}$ is the effective PMA energy, $M_s = (M_s^{\text{Co}} t_{\text{Co}} + M_s^{\text{Ni}} t_{\text{Ni}})/D = 614.3$ emu cm^{-3} is the saturation magnetization, $D = 0.7$ nm is the bilayer thickness, $K_s^{\text{Co/Ni}}$, $K_s^{\text{Ni/Co}}$, $K_s^{\text{Pt/Co}}$, and $K_s^{\text{Ni/Ta}}$ are the interface anisotropy energies of the Co/Ni, Ni/Co, Pt/Co, and Ni/Ta interfaces, respectively. As shown in Fig. 2(d), there is a linear relationship between this energy and $1/n$. Given that $K_s^{\text{Co/Ni}} = K_s^{\text{Ni/Co}}$ and neglecting the $K_s^{\text{Ni/Ta}}$ term, $K_s^{\text{Co/Ni}} = 0.14 \pm 0.01$ (erg cm^{-2}) and $K_s^{\text{Pt/Co}} = 0.57 \pm 0.04$ (erg cm^{-2}) can be obtained. These values are close to what has been previously reported [22,36]. Thus, based on the above-mentioned analysis of crystal structure and interface anisotropy, the samples exhibit clear periodic structures and Co/Pt and Co/Ni interfaces.

III. ANGLE DEPENDENCE OF THE MAGNETORESISTANCE

It is generally believed that the presence of second-order cosine symmetric magnetoresistance in the HM/FM structure in the plane perpendicular to the direction of current [i.e., the yz plane as defined in Fig. 3(a)] is a sign of the SMR [1]. However, in order to strictly separate the contributions of SMR from the geometrical-size effect (GSE) [37,38] and anisotropic interface magnetoresistance (AIMR) [17,18], it is necessary to obtain the thickness dependence of the magnetoresistance in both the xy and yz planes. (See Supplemental Material [39], S3.)

As shown in Fig. 3, we measured the angle-dependent magnetoresistance in the xy and yz planes. A magnetic field of 9 T is applied to ensure that the magnetic moment of the FM is parallel to the magnetic field. Here, α and β denote the angle of the magnetic field direction measured from the x axis in the xy plane and from the z axis in the yz plane. The experimental results of three typical samples are shown in Fig. 3(b). In particular, a $\cos^2\alpha$ behavior is found for all CoNi thicknesses in the xy plane [black circle, Fig. 3(b)], which is consistent with the behavior of conventional AMR. However, the magnetoresistance curve in the yz plane contains higher-order cosine terms and the contribution of this term increases with n. The polar diagram in Fig. 3(d) can be used to further highlight the symmetry of the magnetoresistance in the yz plane. Then, we fit the magnetoresistance curve of the xy plane using the classical AMR equation [33]:

$$\rho(\alpha) = \rho_0 + \Delta\rho_{xy}\cos^2\alpha, \quad (3)$$

where ρ_0 refers to the resistivity when the magnetic field is perpendicular to the current direction, and $\Delta\rho_{xy}$ refers to the change in the resistivity when the magnetic field is aligned with the x- and y axes, respectively. A Fourier analysis reveals that orders of $\cos^{2n}\beta$ have to be considered to properly describe the curves of the yz plane [20]:

$$\rho(\beta) = \rho_0 + \sum_{n=1}^{3} \Delta\rho_{yz}^{(2n)} \cos^{2n}\beta. \qquad (4)$$

This fit the experimental data well, as shown in Fig. 3(c). For all the samples, the sixth-order ($\cos^6\beta$) is much smaller than the other two terms, and therefore, it is omitted from the following discussion.

It is certain that there are various magnetoresistance mechanisms in the Pt/[Co/Ni]$_n$ multilayers. To model the system, we assume that the resistance change due to SMR occurs in Pt whereas the change caused by AIMR and GSE takes place within the CoNi layer. Considering the current shunting effect (see Supplemental Material [39] S1), we can attribute all the magnetoresistance effects in the sample to the contribution of a single magnetic layer. Consequently, different magnetoresistance mechanisms can be identified from the relationship between magnetoresistance and the thickness of the magnetic layer [18,20]. Based on this approach, we consider the shunting effect according to

$$\frac{\Delta\rho_{CoNi}}{\rho_{CoNi}} = \frac{\Delta\rho}{\rho} \times \frac{d_{Pt}\rho_{CoNi} + t_{CoNi}\rho_{Pt}}{t_{CoNi}\rho_{Pt}}, \qquad (5)$$

where $\frac{\Delta\rho}{\rho}$ is the total magnetoresistance, and $\rho_{CoNi} = 1.8 \times 10^{-7}\,\Omega\,m$ and $\rho_{Pt} = 2 \times 10^{-7}\,\Omega\,m$ represent the resistivity of CoNi and Pt.

The SMR effect is derived from the absorption and reflection of the interface spin current in the Pt layer, which is related to the direction of FM magnetization and is reflected as a magnetoresistance under the combined actions of spin Hall effect (SHE) and inverse SHE. There are three basic characteristics of this effect. First, variation of the magnetoresistance depends on the angle between magnetization and spin polarization (y axis), so it can be observed in both the yz and xy planes. Second, according to the previous theory [1], there is only a $\cos^2\beta$ term. Finally, as to what we want to highlight, when the SMR is attributed to the magnetoresistance of the CoNi layer, it will show an inverse relationship with the thickness of the CoNi layer. As shown in Fig. 4(a), the magnetoresistance ratio in the xy plane ($\frac{\Delta\rho_{xy,CoNi}}{\rho_{CoNi}}$) shows a linear dependence with the thickness of $t_{CoNi,corr}$ and is not inversely proportional to the thickness as we expected. Note that $t_{CoNi,corr} = t_{CoNi} - 0.65\,nm$ is the effective thickness of the magnetic layer, where the presence of magnetic dead layers (0.65 nm) at the interface between CoNi and Pt has been considered. (See Supplemental Material [39], S2.) Therefore, this result indicates that SMR may be absent in our samples. Nevertheless, we do observe magnetoresistance in the yz plane, which is usually the basis used to identify SMR. Therefore, we need to further analyze the magnetoresistance observed in the yz plane.

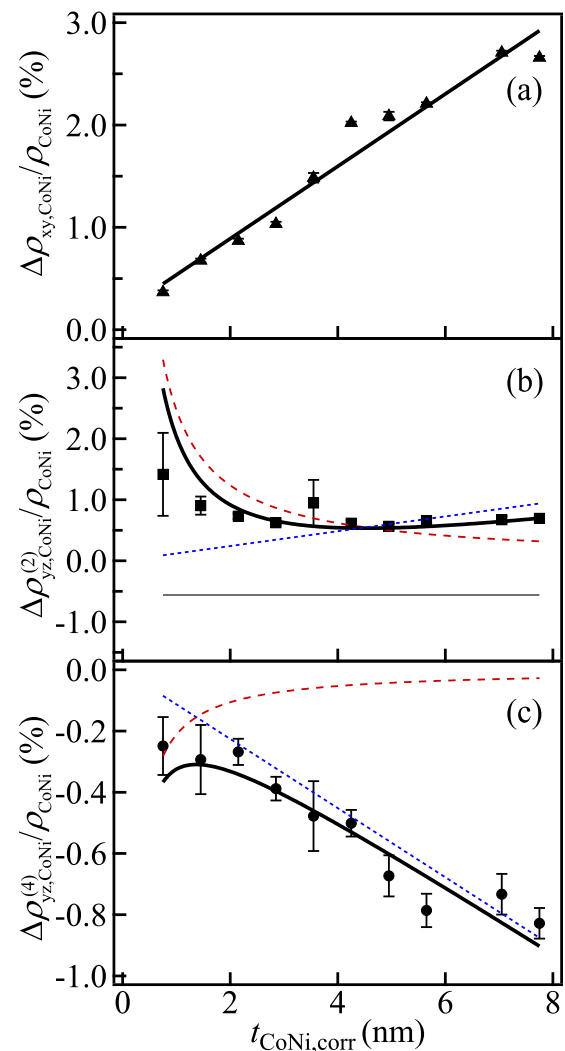Figure 4(b) shows a nonmonotonic change between the second-order magnetoresistance ratio in the yz plane

FIG. 4. The thickness-dependent magnetoresistance after corrections of dead layer. (a) $\Delta\rho_{xy,CoNi}/\rho_{CoNi}$ (b) $\Delta\rho_{yz,CoNi}^{(2)}/\rho_{CoNi}$, and (c) $\Delta\rho_{yz,CoNi}^{(4)}/\rho_{CoNi}$ as a function of the thickness of CoNi. The symbols represent experimental data, while solid black lines represent fitting lines. The dashed red lines represent the contribution of AIMR [the contribution of A in Eq. (6)]. The GSE contribution is a constant that is independent of the thickness [the contribution of C in Eq. (6)], which is indicated by a thinner solid straight line in (b). The blue dotted lines indicate the linear contribution, which corresponds to B in Eq. (6).

($\Delta\rho_{yz,CoNi}^{(2)}/\rho_{CoNi}$) and $t_{CoNi,corr}$. When $t_{CoNi,corr} < 4\,nm$, the magnetoresistance ratio decreases as the thickness increases, thus confirming the existence of an interfacial contribution. When $t_{CoNi,corr} \geqslant 4\,nm$ the magnetoresistance ratio tends to increase with the thickness. Therefore, we fit the thickness dependence of the magnetoresistance ratio using the following empirical formula:

$$\frac{\Delta\rho_{yz,CoNi}^{(2n)}}{\rho_{CoNi}} = \frac{A}{t_{CoNi,corr}} + Bt_{CoNi,corr} + C, \qquad (6)$$

where three undetermined parameters, namely A, B, and C, are introduced. A describes the contribution of the interface, B represents the contribution of the linear relationship with

the thickness, and C represents the contribution independent of the thickness. As shown by the black curve in Fig. 4(b), the fitting formula matches the experimental data, and the fitting results are $A = 0.025$ nm, $B = 0.012$ nm^{-1}, and $C = -0.0006$. Assuming that A entirely comprises SMR contributions, a small percent change in magnetoresistance in the xy plane should have been observed (e.g., $\frac{\Delta\rho_{xy,\mathrm{CoNi}}}{\rho_{\mathrm{CoNi}}}$ should be 2.5% at $t_{\mathrm{CoNi,corr}} = 1$ nm). However, as shown in Fig. 4(a), the magnetoresistance is below 1% when the thickness is less than 2 nm, which further proves that the contribution of SMR can be neglected.

Three primary components contribute to the magnetoresistance of Pt/(CoNi)$_n$ in the yz plane. First, AIMR arises because of the anisotropic interfacial scattering of conductive electrons, which only presents when magnetization varies in the yz plane with high-order cosine terms as shown in the red dashed lines in Figs. 4(b) and 4(c). Second, the negative constant term in the second-order term can be attributed to the GSE effect as indicated by a solid straight line in Fig. 4(b), which is caused by the crystallinity and the anisotropic orientation of the grains [18,20]. Third, the part where there is a linear relationship with the thickness appears in the second-order and fourth-order terms [the blue dotted lines in Figs. 4(b) and 4(c)], and the mechanism for this is still being investigated. In summary, through the above detailed analysis, we proved that SMR was not evident in the samples. Moreover, the presence of a $\cos^2\beta$ magnetoresistance in the yz plane is not the only criterion for determining the existence of SMR.

IV. THEORETICAL PREDICTION OF THE AMPLITUDE OF SMR

To further investigate the absence of SMR, the theoretical value of SMR in the sample needs to be determined. It is well known that when the Pt layer thickness is much larger than its spin-diffusion length, the spin Hall angle (θ_{SH}) is the only key parameter that determines the SMR value [4]. Therefore, based on spin-torque ferromagnetic resonance methods [14,29,42–45], we introduced a microwave signal with a GHz frequency into the Pt/(CoNi)$_n$ microstrip. The measured typical ST-FMR spectrum is shown in Fig. 5(a), and the experimental conditions are 18.5 GHz, 25 dBm, and $\alpha = 45°$. The spectrum can be well fitted with a general line-shape equation as follows:

$$V_{dc} = U_s \frac{\Delta H^2}{\Delta H^2 + (H - H_0)^2} + U_a \frac{\Delta H(H - H_0)}{\Delta H^2 + (H - H_0)^2}, \quad (7)$$

where U_s and U_a are the voltage amplitudes of the symmetric Lorentz and antisymmetric dispersive line shapes, which, according to the theory of Sankey et al., are due to the dampinglike torque caused by SHE of the Pt layer and torque caused by the Oersted field [43], and ΔH and H_0 are the linewidth and resonance field. In order to accurately obtain the spin Hall angle, we first obtained the angular dependence of U_s and U_a, as shown in Fig. 5(b). They all satisfy the theoretical angle-dependence relationship of $\sin 2\alpha \cos\alpha$, which means that the ratio between U_s and U_a is independent of the angle. (See Supplemental Material [39], S4 for the details
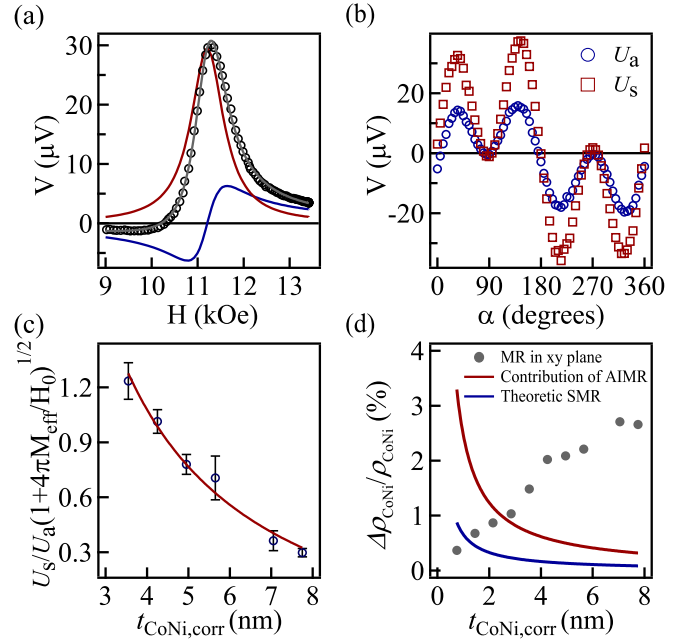

FIG. 5. (a) ST-FMR spectrum of $n = 7$ sample measured at $45°$ in plane with a microwave injection of 18 GHz, which includes antisymmetric (blue curve) and Lorentz symmetric (red curve) line shapes. (b) Angular dependence of U_s and U_a at 18 GHz in the xy plane. (c) Fitting the spin Hall angle (θ_{SH}) according to Eq. (9). (d) The dependence of the xy plane magnetoresistance, the theoretical value of SMR, and the experimental value of AIMR on the thickness of CoNi are put together for comparison.

of the angular-dependent line-shape fitting.) In addition, we measured the U_s/U_a ratio of samples with different CoNi thicknesses at 18 GHz and then fitted according to Eq. (3) in Ref. [43],

$$\frac{U_s}{U_a}\left[1 + \left(\frac{4\pi M_{\mathrm{eff}}}{H_0}\right)\right]^{1/2} = \theta_{\mathrm{SH}} \frac{\hbar}{e\mu_0 M_s t_{\mathrm{CoNi,corr}} d_{\mathrm{Pt}}}. \quad (8)$$

Through the reciprocal relationship with $t_{\mathrm{CoNi,corr}}$, the spin Hall angle of Pt was directly determined to be 0.07. It should be noted that we considered the interface to be transparent to the spin current generated in Pt. If the transparency of the Pt/Co interface $T = 0.65 \pm 0.06$ is considered, according to Ref. [46], the spin current density of Pt flowing to the Co/Pt interface is greater than that flowing into the CoNi layer. Thus, the spin Hall angle in our sample is estimated to be larger than 0.07. The SMR $\sim 7.3 \times 10^{-4}$ estimated by

$$\frac{\Delta\rho_{\mathrm{SMR}}}{\rho_{\mathrm{Pt}}} \sim \theta_{SH}^2 \frac{\lambda_{\mathrm{Pt}}}{d_{\mathrm{Pt}}} \tanh\left(\frac{d_{\mathrm{Pt}}}{2\lambda_{\mathrm{Pt}}}\right)\left[1 - \frac{1}{\cosh\left(\frac{d_{\mathrm{Pt}}}{\lambda_{\mathrm{Pt}}}\right)}\right] \quad (9)$$

should be the theoretical minimum (see Supplemental Material [39], S5) where $\lambda_{\mathrm{Pt}} = 1.5$ nm is the spin-diffusion length of Pt [3].

In order to directly compare the theoretical SMR value with our experimental results, the theoretical SMR value is attributed to the magnetoresistance of the CoNi layer through shunt treatment (see Supplemental Material [39], S1). The theoretical SMR contribution, which is inversely proportional

to the thickness of the CoNi layer in the xy and yz planes, corresponds to $A_{SMR} \approx 6.57 \times 10^{-3}$ nm in Eq. (6). In order to facilitate comparison, the theoretical prediction of SMR, the second-order contribution of AIMR in the experimental data, and the experimental results of the magnetoresistance in the xy plane were all included in Fig. 5(d). It is evident that the theoretical SMR is higher than the experimental value, when the thickness of the CoNi layer is less than 2 nm. This fact indicates that the current experimental accuracy can fully characterize the SMR effect predicted by the theory. Further estimates based on our experimental accuracy suggest that the order of magnitude of SMR in our system should be less than 1×10^{-4}. This value is far less than the values of SMR in metallic systems with Pt = 10 nm that have been reported by others [5,13]. In addition, the magnitude of AIMR is 4 times larger than that of the theoretical SMR. Therefore, even if SMR appears, the magnetoresistance in the yz plane is dominated by the AIMR contribution.

V. RESULTS AND DISCUSSION

The results of the ST-FMR experiment indicate the existence of the spin-orbit torque (SOT). However, such an absorption of spin currents was not evidenced by an apparent SMR. Based on the first model proposed by Chen *et al.* [1], the spin current density $\boldsymbol{j}_s^{(\mathbf{F})}$ at the Pt/YIG (Y$_3$Fe$_5$O$_{12}$) interface is

$$e\boldsymbol{j}_s^{(\mathbf{F})}(\boldsymbol{M}) = G_r \boldsymbol{M} \times (\boldsymbol{M} \times \boldsymbol{\mu}_s) + G_i(\boldsymbol{M} \times \boldsymbol{\mu}_s), \qquad (10)$$

where $G_r(G_i)$ is the real(imaginary) component of the spin-mixing conductance, and $\boldsymbol{\mu}_s$ is the accumulation of spin at the interface. The spin currents absorbed by YIG via SOT and the reflected spin currents are uniquely influenced by the direction of magnetization, which eventually leads to the SMR effect. Based on this model, the SMR and SOT should happen simultaneously. In the following, we try to figure out such a puzzle from the viewpoint of spin transportation in magnetic heterostructures.

Starting from the interface effect, we first consider the spin memory loss (SML) on the spin transport of the Pt/Co interface [47,48]. SML implies that the spin currents flowing into the CoNi layer are significantly lower than that flowing into the Pt/Co interface in Pt. This type of interfacial absorption of the spin current is independent of the $\mathbf{M}$ of the CoNi layer, which may decrease the value of SMR. Nevertheless, SML is equivalent to inserting a spin sink layer (SSL) with a specific thickness and spin-diffusion length between the FM and the HM. The spin current at the interface of SSL/FM is similar to Eq. (10), and the Pt layer and SSL can be combined to form an equivalent HM with a smaller θ_{SH}. As the spin current acting on $\mathbf{M}$ in the FM can be detected using ST-FMR, a lower $\theta_{SH} = 0.07$ than previously reports [49] is consistent with the above discussion. However, the magnitude of SMR estimated using $\theta_{SH} = 0.07$ is still within the range of our experimental accuracy. Therefore, only considering the SML does not reasonably explain our experimental results.

As SMR was first confirmed and systematically studied in HM/YIG, we believe that the SMR effect in HM/FMI and HM/FM is significantly different due to the different carriers

of spin current and the corresponding scattering mechanisms in FMI and FMs [50–52]. In general, spin current can only be absorbed by FMI through the spin angular-momentum exchange between the localized magnetization $\mathbf{M}$ in FMI and the conduction-electron spin polarization $\boldsymbol{\sigma}$ in HMs, i.e., via SOT. However, in FMs, the spin relaxation of itinerant electrons needs to be considered. In 2011, Berger extended Elliott's theory of spin relaxation in normal metals and semiconductors to include metallic ferromagnets [53]. He found that the spin relaxation time is inversely proportional to the spin down resistivity for materials whose spin-up fermi levels are located above the top of the 3d band, such as Ni and Co. Further experimental results confirmed this theory: for instance, Sagasta *et al.* reported that the Elliott-Yafet mechanism is the dominant spin-relaxation mechanism in permalloys [54]; Zhang *et al.* introduced a spin-flip relaxation time to describe the spin transport in FM, and proposed an explicit expression for unidirectional SMR in HM/FM bilayers [55].

With regard to the absence of SMR observed during our experiment, we consider two mechanisms that absorbed the injected spin currents in FMs: SOT ($\mathbf{M}$ dependent, interfacial effect) and spin relaxation (less $\mathbf{M}$ independent, bulk effect). The absorption of spin current using SOT is dominant when $\mathbf{M}$ is perpendicular to $\boldsymbol{\sigma}$. Contrarily, when $\mathbf{M}$ is parallel to $\boldsymbol{\sigma}$, SOT is not applicable, but most of the spin currents would be relaxed in FM according to the mechanism proposed by Berger [53]. In general, a majority of the spin currents flowing into FM will be absorbed, resulting in the spin current at the interface that is independent of (or less dependent on) the direction of magnetization. Therefore, although SOT in the Pt/CoNi system was evident, a corresponding magnitude of SMR does not appear. In conclusion, we believe that when considering addition mechanisms for the spin current absorption in FMs, the expression of the spin current at the HM/FMI interface is inapplicable to the HM/FM interface. As a result, SMR performance would be significantly different.

VI. CONCLUSIONS

In summary, we systematically investigated the magnetoresistance effect in a Pt/(CoNi)$_n$ system with strong PMA and (111) texture. By comparing the magnetoresistance characteristics of the yz and xy planes, we determined that the magnetoresistance with interface characteristics in the yz plane are primarily attributed to AIMR, and no obvious contribution of SMR was found in the experimental results. We obtained the θ_{SH} of Pt through ST-FMR, and the magnitude predicted by the SMR theory was higher than our experimental accuracy. As a consequence, the appearance of $\cos^2\beta$ terms in the plane perpendicular to the current cannot be used as a fingerprint for the presence of SMR. The separation of the magnetoresistance in the yz plane introduced by the symmetry breaking of the interface is a necessary prerequisite for the study of the SMR effect in metallic magnetic heterostructures. Moreover, the itinerant magnetism and the corresponding spin-relaxation mechanisms in FMs would result in the spin currents at HM/FM interface that are less dependent on the magnetization, which is responsible for the absence of SMR in our results.

[1] Y. T. Chen, S. Takahashi, H. Nakayama, M. Althammer, S. T. B. Goennenwein, E. Saitoh, and G. E. W. Bauer, Theory of spin Hall magnetoresistance, Phys. Rev. B **87**, 144411 (2013).

[2] H. Nakayama, M. Althammer, Y. T. Chen, K. Uchida, Y. Kajiwara, D. Kikuchi, T. Ohtani, S. Geprags, M. Opel, S. Takahashi, R. Gross, G. E. Bauer, S. T. Goennenwein, and E. Saitoh, Spin Hall Magnetoresistance Induced By A Nonequilibrium Proximity Effect, Phys. Rev. Lett. **110**, 206601 (2013).

[3] M. Althammer, S. Meyer, H. Nakayama, M. Schreier, S. Altmannshofer, M. Weiler, H. Huebl, S. Geprags, M. Opel, R. Gross, D. Meier, C. Klewe, T. Kuschel, J. M. Schmalhorst, G. Reiss, L. M. Shen, A. Gupta, Y. T. Chen, G. E. W. Bauer, E. Saitoh, and S. T. B. Goennenwein, Quantitative study of the spin Hall magnetoresistance in ferromagnetic insulator/normal metal hybrids, Phys. Rev. B **87**, 224401 (2013).

[4] M. Kawaguchi, D. Towa, Y. C. Lau, S. Takahashi, and M. Hayashi, Anomalous spin Hall magnetoresistance in Pt/Co bilayers, Appl. Phys. Lett. **112**, 202405 (2018).

[5] J. Kim, P. Sheng, S. Takahashi, S. Mitani, and M. Hayashi, Spin Hall Magnetoresistance in Metallic Bilayers, Phys. Rev. Lett. **116**, 097201 (2016).

[6] L. Zhou, H. Song, K. Liu, Z. Luan, P. Wang, L. Sun, S. Jiang, H. Xiang, Y. Chen, J. Du, H. Ding, K. Xia, J. Xiao, and D. Wu, Observation of spin-orbit magnetoresistance in metallic thin films on magnetic insulators, Sci. Adv. **4**, eaao3318 (2018).

[7] X. Z. Chen, R. Zarzuela, J. Zhang, C. Song, X. F. Zhou, G. Y. Shi, F. Li, H. A. Zhou, W. J. Jiang, F. Pan, and Y. Tserkovnyak, Antidamping-Torque-Induced Switching in Biaxial Antiferromagnetic Insulators, Phys. Rev. Lett. **120**, 207204 (2018).

[8] J. Fischer, M. Althammer, N. Vlietstra, H. Huebl, S. T. B. Goennenwein, R. Gross, S. Geprägs, and M. Opel, Large Spin Hall Magnetoresistance in Antiferromagnetic α-Fe$_2$O$_3$/Pt Heterostructures, Phys. Rev. Appl. **13**, 014019 (2020).

[9] J. H. Han, P. X. Zhang, J. T. Hou, S. A. Siddiqui, and L. Q. Liu, Mutual control of coherent spin waves and magnetic domain walls in a magnonic device, Science **366**, 1121 (2019).

[10] J. Fischer, O. Gomonay, R. Schlitz, K. Ganzhorn, N. Vlietstra, M. Althammer, H. Huebl, M. Opel, R. Gross, S. T. B. Goennenwein, and S. Geprags, Spin Hall magnetoresistance in antiferromagnet/heavy-metal heterostructures, Phys. Rev. B **97**, 014417 (2018).

[11] S. Y. Huang, X. Fan, D. Qu, Y. P. Chen, W. G. Wang, J. Wu, T. Y. Chen, J. Q. Xiao, and C. L. Chien, Transport Magnetic Proximity Effects In Platinum, Phys. Rev. Lett. **109**, 107204 (2012).

[12] C. Hahn, G. de Loubens, O. Klein, M. Viret, V. V. Naletov, and J. B. Youssef, Comparative measurements of inverse spin Hall effects and magnetoresistance in YIG/Pt and YIG/Ta, Phys. Rev. B **87**, 174417 (2013).

[13] J. G. Choi, J. W. Lee, and B. G. Park, Spin Hall magnetoresistance in heavy-metal/metallic-ferromagnet multilayer structures, Phys. Rev. B **96**, 174412 (2017).

[14] W. L. Yang, J. W. Wei, C. H. Wan, Y. W. Xing, Z. R. Yan, X. Wang, C. Fang, C. Y. Guo, G. Q. Yu, and X. F. Han, Determining spin-torque efficiency in ferromagnetic metals via spin-torque ferromagnetic resonance, Phys. Rev. B **101**, 064412 (2020).

[15] Y. Yang, Z. Luo, H. Wu, Y. Xu, R. W. Li, S. J. Pennycook, S. Zhang, and Y. Wu, Anomalous Hall magnetoresistance in a ferromagnet, Nat. Commun. **9**, 2255 (2018).

[16] T. Taniguchi, Magnetoresistance generated from charge-spin conversion by anomalous Hall effect in metallic ferromagnetic/nonmagnetic bilayers, Phys. Rev. B **94**, 174440 (2016).

[17] A. Kobs, S. Hesse, W. Kreuzpaintner, G. Winkler, D. Lott, P. Weinberger, A. Schreyer, and H. P. Oepen, Anisotropic Interface Magnetoresistance in Pt/Co/Pt Sandwiches, Phys. Rev. Lett. **106**, 217207 (2011).

[18] A. Kobs and H. P. Oepen, Disentangling interface and bulk contributions to the anisotropic magnetoresistance in Pt/Co/Pt sandwiches, Phys. Rev. B **93**, 014426 (2016).

[19] L. K. Zou, Y. Zhang, L. Gu, J. W. Cai, and L. Sun, Tunable angular-dependent magnetoresistance correlations in magnetic films and their implications for spin hall magnetoresistance analysis, Phys. Rev. B **93**, 075309 (2016).

[20] A. Philippi-Kobs, A. Farhadi, L. Matheis, D. Lott, A. Chuvilin, and H. P. Oepen, Impact of Symmetry on Anisotropic Magnetoresistance in Textured Ferromagnetic Thin Films, Phys. Rev. Lett. **123**, 137201 (2019).

[21] S. Andrieu, T. Hauet, M. Gottwald, A. Rajanikanth, L. Calmels, A. M. Bataille, F. Montaigne, S. Mangin, E. Otero, P. Ohresser, P. Le Fevre, F. Bertran, A. Resta, A. Vlad, A. Coati, and Y. Garreau, Co/Ni multilayers for spintronics: High spin polarization and tunable magnetic anisotropy, Phys. Rev. Mater. **2**, 064410 (2018).

[22] L. You, R. C. Sousa, S. Bandiera, B. Rodmacq, and B. Dieny, Co/Ni multilayers with perpendicular anisotropy for spintronic device applications, Appl. Phys. Lett. **100**, 172411 (2012).

[23] M. Haertinger, C. H. Back, S. H. Yang, S. S. P. Parkin, and G. Woltersdorf, Properties of Ni/Co multilayers as a function of the number of multilayer repetitions, J. Phys. D: Appl. Phys. **46**, 175001 (2013).

[24] V. Ostwal, A. Penumatcha, Y. M. Hung, A. D. Kent, and J. Appenzeller, Spin-orbit torque based magnetization switching in Pt/Cu/[Co/Ni]$_5$ multilayer structures, J. Appl. Phys. **122**, 213905 (2017).

[25] S. Mangin, D. Ravelosona, J. A. Katine, M. J. Carey, B. D. Terris, and E. E. Fullerton, Current-induced magnetization reversal in nanopillars with perpendicular anisotropy, Nat. Mater. **5**, 210 (2006).

[26] J. Yu, X. Qiu, Y. Wu, J. Yoon, P. Deorani, J. M. Besbas, A. Manchon, and H. Yang, Spin orbit torques and Dzyaloshinskii-Moriya interaction in dual-interfaced Co-Ni multilayers, Sci. Rep. **6**, 32629 (2016).

[27] S. Mizukami, X. M. Zhang, T. Kubota, H. Naganuma, M. Oogane, Y. Ando, and T. Miyazaki, Gilbert damping in Ni/Co

multilayer films exhibiting large perpendicular anisotropy, Appl. Phys. Express **4**, 013005 (2011).

[28] H. S. Song, K. D. Lee, J. W. Sohn, S. H. Yang, S. S. P. Parkin, C. Y. You, and S. C. Shin, Observation of the intrinsic Gilbert damping constant in Co/Ni multilayers independent of the stack number with perpendicular anisotropy, Appl. Phys. Lett. **102**, 102401 (2013).

[29] J. M. L. Beaujour, W. Chen, K. Krycka, C. C. Kao, J. Z. Sun, and A. D. Kent, Ferromagnetic resonance study of sputtered Co|Ni multilayers, Eur. Phys. J. B **59**, 475 (2007).

[30] B. Tudu and A. Tiwari, Recent developments in perpendicular magnetic anisotropy thin films for data storage applications, Vacuum **146**, 329 (2017).

[31] M. Seddat, M. Tessier, R. Krishnan, H. Lassri, S. Visnovsky, S. K. Kulkarni, and M. Vedpathak, Difference in the behaviour of interfacial Co and Ni atoms in Co_xNi_{1-x}/Pt multilayers: an explanation, J. Phys. D: Appl. Phys. **33**, 1662 (2000).

[32] M. Arora, R. Hubner, D. Suess, B. Heinrich, and E. Girt, Origin of perpendicular magnetic anisotropy in Co/Ni multilayers, Phys. Rev. B **96**, 024401 (2017).

[33] T. McGuire and R. Potter, Anisotropic magnetoresistance in ferromagnetic 3d alloys, IEEE Trans. Magn. **11**, 1018 (1975).

[34] P. Zhang, K. Xie, W. Lin, D. Wu, and H. Sang, Anomalous Hall effect in Co/Ni multilayers with perpendicular magnetic anisotropy, Appl. Phys. Lett. **104**, 082404 (2014).

[35] Y. Chen, Q. Zhang, J. Jia, Y. Zheng, Y. Wang, X. Fan, and J. Cao, Tuning Slonczewski-like torque and Dzyaloshinskii–Moriya interaction by inserting a Pt spacer layer in Ta/CoFeB/MgO structures, Appl. Phys. Lett. **112**, 232402 (2018).

[36] M. T. Johnson, P. J. H. Bloemen, F. J. A. den Broeder, and J. J. de Vries, Magnetic anisotropy in metallic multilayers, Rep. Prog. Phys. **59**, 1409 (1996).

[37] T. T. Chen and V. A. Marsocci, Transverse magnetoresistivity anisotropy measurements and the geometrical size effect in nickel thin films, J. Appl. Phys. **43**, 1554 (1972).

[38] W. Gil, D. Gorlitz, M. Horisberger, and J. Kotzler, Magnetoresistance anisotropy of polycrystalline cobalt films: Geometrical-size and domain effects, Phys. Rev. B **72**, 134401 (2005).

[39] See Supplemental Material at http://link.aps.org/supplemental/10.1103/PhysRevB.103.024415 for the details of shunting effect, determining the dead layer thickness, angular-dependent magnetoresistance in three planes, angular-dependent lineshape fitting, and estimating the minimum value of SMR, which includes Refs. [40,41].

[40] V. P. Amin, J. Zemen, and M. D. Stiles, Interface-Generated Spin Currents, Phys. Rev. Lett. **121**, 136805 (2018).

[41] T. Horaguchi, M. Matsuo, and Y. Nozaki, Highly accurate evaluation of spin-torque efficiency by measuring in-plane angular dependence of spin-torque ferromagnetic resonance, J. Magn. Magn. Mater. **505**, 166727 (2020).

[42] W. W. Kong, X. L. Fan, H. G. Zhou, J. W. Cao, D. W. Guo, Y. S. Gui, C. M. Hu, and D. S. Xue, Electrical detec-

tion of magnetization dynamics in an ultrathin CoFeB film with perpendicular anisotropy, Appl. Phys. Lett. **109**, 182406 (2016).

[43] L. Liu, T. Moriyama, D. C. Ralph, and R. A. Buhrman, Spin-Torque Ferromagnetic Resonance Induced By The Spin Hall Effect, Phys. Rev. Lett. **106**, 036601 (2011).

[44] J. C. Sankey, Y.-T. Cui, J. Z. Sun, J. C. Slonczewski, R. A. Buhrman, and D. C. Ralph, Measurement of the spin-transfer-torque vector in magnetic tunnel junctions, Nat. Phys. **4**, 67 (2007).

[45] Q. H. Zhang, Y. F. Chen, Y. D. Zheng, J. W. Cao, D. S. Xue, and X. L. Fan, The positive correlation between interface Dzyaloshinskii-Moriya interaction and damping-like spin Hall torque in the Ta/Pt/CoFeB/MgO/Ta system, Appl. Phys. Express **12**, 103001 (2019).

[46] W. Zhang, W. Han, X. Jiang, S.-H. Yang, and S. S. P. Parkin, Role of transparency of platinum–ferromagnet interfaces in determining the intrinsic magnitude of the spin Hall effect, Nat. Phys. **11**, 496 (2015).

[47] K. Gupta, R. J. H. Wesselink, R. Liu, Z. Yuan, and P. J. Kelly, Disorder Dependence of Interface Spin Memory Loss, Phys. Rev. Lett. **124**, 087702 (2020).

[48] J. C. Rojas-Sánchez, N. Reyren, P. Laczkowski, W. Savero, J. P. Attané, C. Deranlot, S. Gambarelli, M. Jamet, J. M. George, L. Vila, and H. Jaffrès, Spin pumping and inverse spin Hall effect in platinum and other 5d metals: The essential role of spin-memory loss and spin-current discontinuities at interfaces, Proc. SPIE **9167**, 916729 (2014).

[49] X. D. Tao, Q. Liu, B. F. Miao, R. Yu, Z. Feng, L. Sun, B. You, J. Du, K. Chen, S. F. Zhang, L. Zhang, Z. Yuan, D. Wu, and H. F. Ding, Self-consistent determination of spin Hall angle and spin diffusion length in Pt and Pd: The role of the interface spin loss, Sci. Adv. **4**, 2375 (2018).

[50] X. G. Wang, Z. X. Li, Z. W. Zhou, Y. Z. Nie, Q. L. Xia, Z. M. Zeng, L. Chotorlishvili, J. Berakdar, and G. H. Guo, Conversion of electronic to magnonic spin current at a heavy-metal magnetic-insulator interface, Phys. Rev. B **95**, 020414(R) (2017).

[51] X. G. Wang, Z. W. Zhou, Y. Z. Nie, Q. L. Xia, and G. H. Guo, Self-consistent study of local and nonlocal magnetoresistance in a YIG/Pt bilayer, Phys. Rev. B **97**, 094401 (2018).

[52] S. Zhang and Z. Li, Roles of Nonequilibrium Conduction Electrons on the Magnetization Dynamics Of Ferromagnets, Phys. Rev. Lett. **93**, 127204 (2004).

[53] L. Berger, Spin relaxation in metallic ferromagnets, Phys. Rev. B **83**, 054410 (2011).

[54] E. Sagasta, Y. Omori, M. Isasa, Y. Otani, L. E. Hueso, and F. Casanova, Spin diffusion length of permalloy using spin absorption in lateral spin valves, Appl. Phys. Lett. **111**, 082407 (2017).

[55] S. S. L. Zhang and G. Vignale, Theory of unidirectional spin Hall magnetoresistance in heavy-metal/ferromagnetic-metal bilayers, Phys. Rev. B **94**, 140411(R) (2016).